

Modeling the Distributed MU-MIMO OAI 5G testbed and group-based OTA calibration performance evaluation

Theoni Magounaki
EURECOM
 Sophia Antipolis, France
 theoni.magounaki@eurecom.fr

Florian Kaltenberger
EURECOM
 Sophia Antipolis, France
 florian.kaltenberger@eurecom.fr

Raymond Knopp
EURECOM
 Sophia Antipolis, France
 raymond.knopp@eurecom.fr

Abstract—In this paper we describe the simulation modeling of the OpenAirInterface (OAI) C-RAN testbed deployed at Eurecom and present the performance evaluation of a fast calibration (FC) scheme based on antenna grouping. We generate an indoor LOS radio wave propagation model using ray tracing technique and perform distributed channel reciprocity calibration which is required to exploit uplink (UL) channel estimates to infer the precoder performed on the downlink (DL) channel. We consider a channel based on the geometry of the area where the RRUs are distributed and compare the different choices to form the RRU groups. We validate that the simulation results match the experimental results from our previous work [1].

Index Terms—channel reciprocity calibration, distributed antenna system, TDD, Massive MIMO, C-RAN

I. INTRODUCTION

Massive multiple input multiple output (MIMO), is an extension of multi-user MIMO, which uses an order of magnitude more antennas than classical MIMO systems and improves the end user experience by significantly increasing network capacity and coverage while also reducing interference. The “massive” number of antennas helps focus energy, bringing huge improvements in throughput and radiated energy efficiency. Massive MIMO is a key enabler of 5G’s extremely fast data rates and relies on uplink pilots to obtain channel state information (CSI), exploiting channel reciprocity and time division duplexing (TDD) operation.

Distributed antenna systems (DAS) have been introduced as a key technology for next generation communications for expanding indoor coverage and increasing sum rates [2], [3], [4]. In DAS we may treat the remote radio units (RRUs) which are spatially separated throughout a cell as a distributed antenna array. Therefore, the average distance between user and transmitter along with the multi-user interference and transmit power can be reduced, resulting in improved overall performance and more uniform coverage [5], [6], [7]. The radio access system of spatially separate RRUs is connected to a central server via a wired backhaul network.

Distributed massive MIMO obtains the best of both worlds: multi-user interference suppression through spatial precoding,

This work has been funded by the french FUI project MASS-START (www.mass-start.fr).

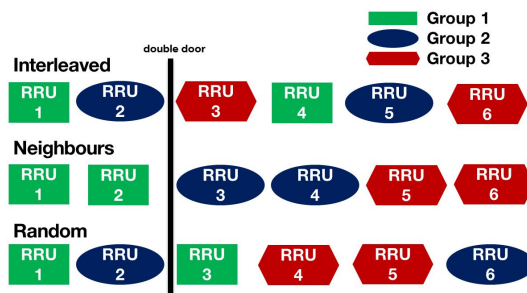


Fig. 1: Example of three different choices to form the RRU groups for M=6 RRUs.

and dense coverage by reducing the average distance between transmitters and receivers. This is achieved by coordinating a large number of RRUs, distributed over a certain coverage region, through a wired backhaul network connected to a central server, forming a cloud radio access network (C-RAN).

A key factor for enabling reciprocity-based distributed massive MIMO is to compensate for the hardware non-symmetry at the transceiver radio frequency (RF) chains. Various calibration solutions to address this problem at the base station (BS) side exist (e.g. Argos [8], Rogalin et al. [9], Avalanche [10]). The authors in [11] presented a fast calibration (FC) scheme based on antenna grouping which outperforms the existing relative calibration algorithms.

In [1], we adapted this to our OAI C-RAN testbed in order to confirm its efficiency, in real environment. We examined the performance results from three different grouping schemes (Interleaved, Neighbours, Random) according to Fig. 1. We illustrated that the interleaved grouping of the RRUs results in performance gains. Furthermore, we played around with the size of the largest group and simultaneously formed groups by selecting RRUs in an interleaving way like in Fig. 2. This proved that the overall estimation performance of the group-based FC algorithm improves when we try to minimize the size of the largest RRU group. These conclusions we made based on the variance of the time-domain calibration elements.

The scope of the present paper is to provide a ground

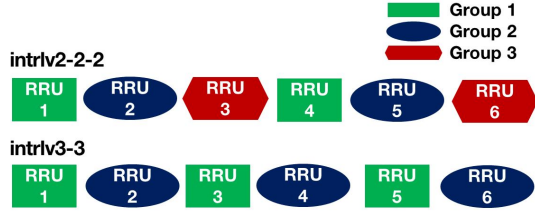


Fig. 2: Example of two different grouping sizes in an interleaving way for $M=6$ RRUs.



Fig. 3: OpenAirInterface 5G testbed

truth for the evaluation of the group-based OTA calibration framework through channel measurements on our simulated distributed antenna system.

The rest of this paper is organized as follows. Section II describes the system architecture of our testbed. In Section III, we present the TDD reciprocity system model and the fast calibration (FC) scheme based on antenna grouping. Section IV explains the estimation of propagation metrics. In Section V, we evaluate the performance of the group-based FC method using the mean square error (MSE) as a metric. Conclusions are drawn in Section VI.

II. SYSTEM ARCHITECTURE

Eurecom deployed a cloud radio access network (C-RAN) network using OpenAirInterface (OAI) software and inexpensive commodity hardware, Fig. 3 [12]. The testbed consists of the following 3 main entities: (i) The remote radio unit (RRU) which is a radio transceiver and contains the RF processing circuitry. (ii) The radio aggregation unit (RAU) which connects multiple RRUs to a baseband unit (BBU) and serves as a data processing unit. (iii) The radio cloud center (RCC) which is responsible for the centralized baseband processing and controls multiple RAUs.

A set of 20 RRUs is deployed on the ceilings of the corridors on levels -3 and -4 of the Eurecom building. The RRUs on each floor are connected by Gbit Ethernet to a switch which are in turn connected to a central server over optical 20 Gbit Ethernet. A frequency reference unit outputs ten high-precision 40 MHz frequency reference outputs on each floor. The RRUs consist of an UP board from Intel, a B200 mini from Ettus Research, a RF frontend designed by Eurecom and Power over Ethernet (PoE) technology.

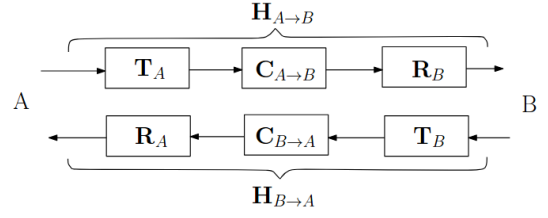


Fig. 4: Reciprocity Model

III. RELATIVE CALIBRATION SCHEME

TDD reciprocity calibration is one of the key factors to enable distributed multi-user MIMO. In this section we review the relative calibration scheme from [11].

We consider a TDD communication system involving a BS A and a UE B with M_A antennas and M_B antennas respectively, illustrated in Fig. 4. The channel seen by transceivers in the digital domain (the composite channel), is comprised of the physical channel \mathbf{C} , assumed reciprocal in both UL and DL, and filters modeling the imperfections of the transmit RF hardware (e.g., power amplifiers (PA)), (\mathbf{T}_A and \mathbf{T}_B), and the receive RF hardware (e.g, low-noise amplifiers (LNA)), (\mathbf{R}_A and \mathbf{R}_B). The diagonal elements represent the gains on each transmit chain whereas the off-diagonal elements correspond to the RF chain on-chip crosstalk and the antenna mutual coupling. We consider the ideal case, where the transmit/receive RF hardware are all diagonal filters (no crosstalk/mutual coupling) and carrier frequency at both sides is identical. Also, the filters modeling the amplifiers are assumed to remain constant over the observed quite long time horizon. The measured UL and DL channels between nodes A and B, represented by $\mathbf{H}_{A \rightarrow B}$ and $\mathbf{H}_{B \rightarrow A}$, are thus modeled as:

$$\begin{aligned} \mathbf{H}_{A \rightarrow B} &= \mathbf{R}_B \mathbf{C}_{A \rightarrow B} \mathbf{T}_A \\ \mathbf{H}_{B \rightarrow A} &= \mathbf{R}_A \mathbf{C}_{B \rightarrow A} \mathbf{T}_B \end{aligned} \quad (1)$$

Since we operate within the channel coherence time we can eliminate the physical channel \mathbf{C} from (1) and we obtain:

$$\mathbf{H}_{A \rightarrow B} = \mathbf{F}_B^{-T} \mathbf{H}_{B \rightarrow A}^T \mathbf{F}_A \quad (2)$$

where $\mathbf{F}_A = \mathbf{R}_A^{-T} \mathbf{T}_A$ and $\mathbf{F}_B = \mathbf{R}_B^{-T} \mathbf{T}_B$ include the hardware properties and are called the *calibration matrices*.

OTA calibration relies on signal processing techniques to calibrate at RF chain level and compensate the hardware non-symmetry. Thus, we estimate \mathbf{F}_A and \mathbf{F}_B which along with the UL channel estimates $\mathbf{H}_{B \rightarrow A}$ give us the CSIT $\mathbf{H}_{A \rightarrow B}$, (2), based on which advanced beamforming techniques can be implemented. In [13] it is shown that the RF mismatches for degrading the system's performance. Hence, we perform *partial calibration* which is part of the relative or over-the-air (OTA) calibration methods. In partial calibration only the RF mismatches at the BS are calibrated. This has no impact at the beamforming performance as any unknown complex scalar

factor is compensated by the channel estimation at the UE. We thus, in the sequel, focus on the estimation of \mathbf{F}_A , although the framework discussed in the following is not limited to this case.

Let us describe how the calibration matrix \mathbf{F}_A is estimated based on the fast calibration scheme proposed in [11]. We consider a set of M RRUs partitioned into G groups denoted by A_1, A_2, \dots, A_G , as in Fig. 5. Group A_i contains M_i RRUs such that $\sum_{i=1}^G M_i = M$. Each group A_i transmits a sequence of L_i pilot symbols, defined by matrix $\mathbf{P}_i \in \mathbb{C}^{M_i \times L_i}$ where the rows correspond to antennas and the columns to successive channel uses. A channel use is considered as a calibration symbol or a frame. When an antenna group i transmits, all other groups are considered in receiving mode. After all G groups have transmitted, the received signal for each resource block of bidirectional transmission between antenna groups i and j is given by

$$\begin{aligned} \mathbf{Y}_{i \rightarrow j} &= \mathbf{R}_j \mathbf{C}_{i \rightarrow j} \mathbf{T}_i \mathbf{P}_i + \mathbf{N}_{i \rightarrow j} \\ \mathbf{Y}_{j \rightarrow i} &= \mathbf{R}_i \mathbf{C}_{j \rightarrow i} \mathbf{T}_j \mathbf{P}_j + \mathbf{N}_{j \rightarrow i} \end{aligned} \quad (3)$$

where $\mathbf{Y}_{i \rightarrow j} \in \mathbb{C}^{M_j \times L_i}$ and $\mathbf{Y}_{j \rightarrow i} \in \mathbb{C}^{M_i \times L_j}$ are received signal matrices at antenna groups j and i respectively. $\mathbf{N}_{i \rightarrow j}$ and $\mathbf{N}_{j \rightarrow i}$ represent the corresponding received noise matrix. \mathbf{T}_i , $\mathbf{R}_i \in \mathbb{C}^{M_i \times M_i}$ and \mathbf{T}_j , $\mathbf{R}_j \in \mathbb{C}^{M_j \times M_j}$ represent the effect of the transmit and receive RF front-ends of antenna elements in groups i and j respectively.

The reciprocity property induces that $\mathbf{C}_{i \rightarrow j} = \mathbf{C}_{j \rightarrow i}^T$, thus for two different groups $1 \leq i \neq j \leq G$ in (3), by eliminating $\mathbf{C}_{i \rightarrow j}$ we have

$$\mathbf{P}_i^T \mathbf{F}_i^T \mathbf{Y}_{j \rightarrow i} - \mathbf{Y}_{i \rightarrow j}^T \mathbf{F}_j \mathbf{P}_j = \tilde{\mathbf{N}}_{ij} \quad (4)$$

The calibration matrix \mathbf{F} is diagonal and thus we can consider $\mathbf{F}_i = \text{diag}\{\mathbf{f}_i\}$ and $\mathbf{F} = \text{diag}\{\mathbf{f}\}$. This allows us to vectorize (4) into

$$(\mathbf{Y}_{j \rightarrow i}^T * \mathbf{P}_i^T) \mathbf{f}_i - (\mathbf{P}_j^T * \mathbf{Y}_{i \rightarrow j}^T) \mathbf{f}_j = \tilde{\mathbf{n}}_{ij} \quad (5)$$

where $*$ denotes the Khatri-Rao product, where we have used the equality $\text{vec}(\mathbf{A} \text{diag}(\mathbf{x}) \mathbf{B}) = (\mathbf{B}^T * \mathbf{A}) \mathbf{x}$. Stacking equations (5) for all $1 \leq i < j \leq G$ yields

$$\mathcal{Y}(\mathbf{P}) \mathbf{f} = \tilde{\mathbf{n}} \quad (6)$$

with $\mathcal{Y}(\mathbf{P})$ defined as

$$\underbrace{\begin{bmatrix} (\mathbf{Y}_{2 \rightarrow 1}^T * \mathbf{P}_1^T) & -(\mathbf{P}_2^T * \mathbf{Y}_{1 \rightarrow 2}^T) & 0 & \cdots \\ (\mathbf{Y}_{3 \rightarrow 1}^T * \mathbf{P}_1^T) & 0 & -(\mathbf{P}_3^T * \mathbf{Y}_{1 \rightarrow 3}^T) & \cdots \\ 0 & (\mathbf{Y}_{3 \rightarrow 2}^T * \mathbf{P}_2^T) & -(\mathbf{P}_3^T * \mathbf{Y}_{2 \rightarrow 3}^T) & \cdots \\ \vdots & \vdots & \vdots & \ddots \end{bmatrix}}_{(\sum_{j=2}^G \sum_{i=1}^{j-1} L_i L_j) \times M} \quad (7)$$

The estimation of the calibration coefficients \mathbf{f} consists in solving a LS problem assuming a unit norm constraint such as

$$\hat{\mathbf{f}} = \arg \min_{\mathbf{f}: \|\mathbf{f}\|=1} \|\mathcal{Y}(\mathbf{P}) \mathbf{f}\|^2 = V_{\min}(\mathcal{Y}(\mathbf{P})^H \mathcal{Y}(\mathbf{P})) \quad (8)$$

where $V_{\min}(\mathbf{X})$ denotes the eigenvector of matrix \mathbf{X} corresponding to its eigenvalue with the smallest magnitude.

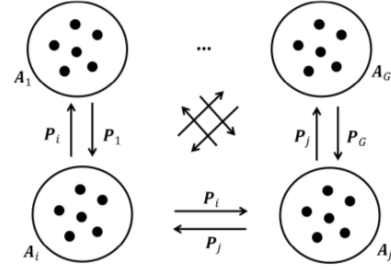


Fig. 5: Bi-directional transmission between antenna groups.

IV. SIMULATED PERFORMANCE ANALYSIS

In order to find the optimal grouping policy for our testbed we carry out simulations. To conduct performance comparisons for different grouping calibration schemes, we use the MSE of calibrated channel matrices as our metric.

$$\text{MSE} = \frac{\mathbb{E} \left[\|\hat{\mathbf{f}} - \mathbf{f}\|^2 \right]}{M - 1} \quad (9)$$

We fix the noise variance to the thermal noise of one subcarrier (15kHz) at $N_0 = -132\text{dBm}$. Thus, the performance of different grouping methods is only driven by the different values at the transmit power per RRU.

A. Channel Model

In the case of indoor radio wave propagation along the corridor of a building, the free space path, ground and side wall reflective path are taken into consideration. The RRU positions are represented in the 3-dimensional space by means of three coordinates (i.e. inter-RRU distance, side wall distance, ceiling height). The inter-RRU distance is set to 5.5m, the distance of each RRU to the side wall is measured at 1.25m, while the ceiling height is 3m. We consider the 2-ray model with LOS and one dominant reflection from the ground.

The path loss depends on whether we are in LOS or NLOS conditions. In the NLOS case we take into account only the reflected ray and we assume a reflection coefficient of -1 . Whereas, in LOS conditions we have to compute the phase difference between the direct ray and the reflected ray, since the received signal may suffer constructive or destructive interference.

The channel (amplitude and phase) between RRU m and n is

- NLOS case

$$c'_{m,n} = -\frac{\lambda}{4\pi d_{\text{ref}}} e^{-jk d_{\text{ref}}} \quad (10)$$

- LOS case

$$c'_{m,n} = \frac{\lambda}{4\pi d_{\text{dir}}} \left(1 - e^{-jk(d_{\text{ref}} - d_{\text{dir}})} \right) \quad (11)$$

where λ is the wave length and $k = \frac{2\pi}{\lambda}$ is the wave number.

In addition to the direct and reflected ray, we also account for diffuse components by adding a random phase $g_{m,n}$ drawn

from a Rayleigh distribution $\mathcal{CN}(0, 1)$ and scaled by a Rician K -factor K .

$$c_{m,n} = \sqrt{K}c'_{m,n} + \sqrt{1-K}g_{m,n}. \quad (12)$$

In our simulations we assume a Rician K -factor for indoor channels of 4dB.

B. Hardware properties model

The reciprocal values T_A and R_A are modeled as i.i.d. random variables, with independent magnitude uniformly distributed on $[1 - \epsilon, 1 + \epsilon]$, with ϵ chosen such that the standard deviation of the squared-magnitudes is 0.1, and uniformly distributed phase between $[-\pi, \pi]$, [14]. We fix the first reciprocal coefficients to 1 ($f_1 = 1$). The transmitted pilots are generated by the same set of base sequences used for physical uplink shared channel demodulation reference signal (PUSCH DMRS) [15]. The modulation type used is Zadoff-Chu, causing the constellation for pilots to look like irregularly spaced points on a circle with unit power. The Zadoff-Chu sequence values are modulated directly onto the subcarriers using OFDM.

C. Simulation Results

We assess numerically the performance of the proposed group-based fast calibration method from Section III at 2.58 GHz. We use the MSE of the calibrated channel normalized by the total number of active RRUs. Some important parameters that impact the MSE of the calibration coefficient estimates are evaluated.

Fig. 6a illustrates the performance results from the three different grouping schemes. The MSE curve with the ‘‘Interleaved’’ grouping method shows that the interleaving of the RRUs ensures that the channel from a group to the rest of the RRUs is as well conditioned as possible. Through our simulations we noticed how crucial is the geometry of the environment to the effective calibration coefficients estimation. For this experiment we consider 6 RRUs in row and a double door blocking the first two RRUs from the rest like in Fig. 1. Changing the inter-RRU distance $d_{i,j}$ by only 1cm may result in destructive interference among almost all the possible pairs of RRUs based on our 2-ray interference channel model. Thus, the benefits of our proposed ‘‘Interleaved’’ grouping scheme no longer hold, Fig. 6b.

Furthermore, in Fig. 7, we verify the fact that the performance improves when the group sizes are allocated more equitably to the minimum group size as in grouping scheme 2-2-2-2-2-2. This can be verified by looking at the condition number of $\mathcal{Y}(\mathbf{P})$ in (7). The condition number of matrices plays an important role in solving systems of linear equations such as the linear least squares method. It measures the sensitivity of the solution of a problem to data quality. It provides an approximate upper bound on the error in a computed solution. In 6-6 scheme, the matrix can be poorly conditioned for inversion so it is more sensitive to machine’s relative round-off errors made during the LS solution process, Fig. 8. Also, we can clearly see from the curves representing

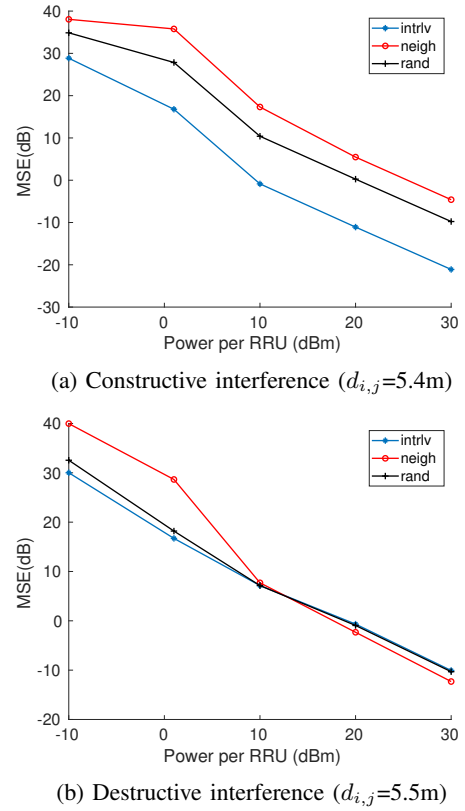


Fig. 6: MSE of estimated calibration matrix over transmit power per RRU ($M=6$ RRUs).

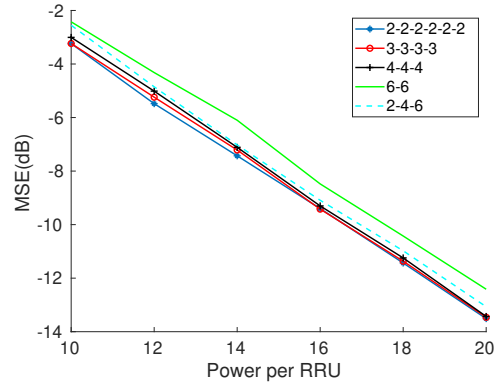


Fig. 7: MSE of estimated calibration matrix over transmit power per RRU (interleaving $M=12$ RRUs - LOS case).

4-4-4 and 2-4-6 that even if we split the RRUs into the same number of groups, grouping them equitably is favorable.

The results presented at Fig. 9 show how strongly a condition number depends on the size of the matrix. Increasing the number of RRUs results in larger linear system of equations and consequently a more accurate approximation of the LS solution. The curves show that the matrices representing the largest possible grouping, the condition number of which is very high, are ill-conditioned, so the LS estimation process

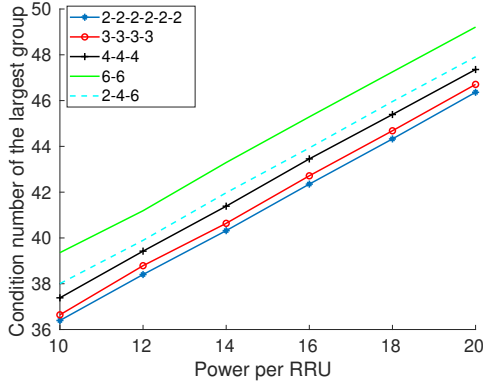


Fig. 8: Condition number of 5 different grouping schemes over transmit power per RRU (interleaving M=12 RRUs - LOS case).

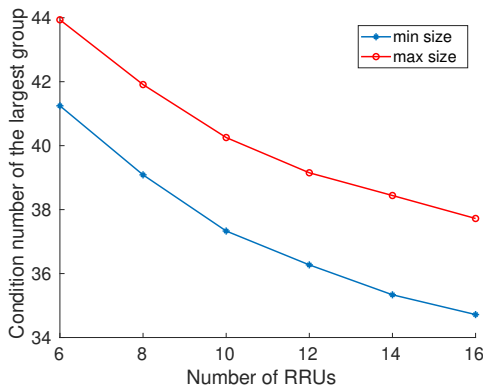


Fig. 9: Condition number of the largest grouping over the total number of distributed RRUs (LOS case).

can generate solutions with a large error, resulting in a calibration matrix with poor accuracy. On the contrary, the matrices formed by the minimum-size grouping scheme, have smaller condition numbers, which means that they are well-conditioned matrices for which the LS estimation process, after a few iterations, gives the estimate with a minor error.

V. CONCLUSIONS

In this work we presented an OTA group-based fast calibration framework and through simulation measurements on our modeled DAS testbed, we performed distributed channel reciprocity calibration. Our results illustrated that the group-based FC with interleaved groups of RRUs results in performance gains. Fig. 6a verifies our assumption that the interleaving of the RRUs ensures a well-conditioned channel from a group to the rest of the RRUs made in [1]. However, the performance of each grouping scheme is highly sensitive to the geometrical characteristics of the area where the RRUs are distributed. Moreover, we proved, through MSE and condition number metrics, that the overall estimation performance of our group-based FC algorithm improves when we try to minimize the size of the largest RRU group with equally partitioned groups. In

Fig. 7 we establish the correctness of the corresponding real-time evaluation made in [1] using variance as a metric.

REFERENCES

- [1] T. Magounaki, F. Kaltenberger, and R. Knopp, "Real-time performance evaluation of relative calibration on the OAI 5G testbed," in *ASILOMAR 2019, Asilomar Conference on Signals, Systems, and Computers*, 3-6 November 2019, Pacific Grove, CA, USA, Pacific Grove, UNITED STATES, 11 2019. [Online]. Available: <http://www.eurecom.fr/publication/6054>
- [2] A. A. M. Saleh, A. Rustako, and R. Roman, "Distributed antennas for indoor radio communications," *IEEE Transactions on Communications*, vol. 35, no. 12, pp. 1245–1251, December 1987.
- [3] S. Zhou, M. Zhao, X. Xu, J. Wang, and Y. Yao, "Distributed wireless communication system: a new architecture for future public wireless access," *IEEE Communications Magazine*, vol. 41, no. 3, pp. 108–113, 2003.
- [4] K. J. Kerpez, "A radio access system with distributed antennas," *IEEE Transactions on Vehicular Technology*, vol. 45, no. 2, pp. 265–275, 1996.
- [5] W. Roh, "High performance distributed antenna cellular networks." Ph.D. dissertation, Stanford University, 2004.
- [6] H. Dai, H. Zhang, and Q. Zhou, "Some analysis in distributed MIMO systems," *JCM*, vol. 2, no. 3, pp. 43–50, 2007.
- [7] W. Choi and J. G. Andrews, "Downlink performance and capacity of distributed antenna systems in a multicell environment," *IEEE Transactions on Wireless Communications*, vol. 6, no. 1, pp. 69–73, 2007.
- [8] C. Shepard, H. Yu, N. Anand, E. Li, T. Marzetta, R. Yang, and L. Zhong, "Argos: Practical many-antenna base stations," in *Proceedings of the 18th annual international conference on Mobile computing and networking*. ACM, 2012, pp. 53–64.
- [9] R. Rogalin, O. Y. Bursalioglu, H. Papadopoulos, G. Caire, A. F. Molisch, A. Michaloliakos, V. Balan, and K. Psounis, "Scalable synchronization and reciprocity calibration for distributed multiuser mimo," *IEEE Transactions on Wireless Communications*, vol. 13, no. 4, pp. 1815–1831, 2014.
- [10] H. Papadopoulos, O. Y. Bursalioglu, and G. Caire, "Avalanche: Fast RF calibration of massive arrays," in *2014 IEEE Global Conference on Signal and Information Processing (GlobalSIP)*. IEEE, 2014, pp. 607–611.
- [11] X. Jiang, A. Decunring, K. Gopala, F. Kaltenberger, M. Guillaud, D. Stock, and L. Deneire, "A framework for over-the-air reciprocity calibration for TDD massive MIMO systems," *IEEE Transactions on Wireless Communications*, vol. 17, no. 9, pp. 5975–5990, Sep. 2018. [Online]. Available: <http://arxiv.org/abs/1710.10830>
- [12] F. Kaltenberger, X. Jiang, and R. Knopp, "From massive MIMO to C-RAN: the OpenAirInterface 5G testbed," in *Proceeding of Asilomar Conference on Signals, Systems, and Computers*, Pacific Grove, CA, Oct. 2017.
- [13] H. Wei, D. Wang, H. Zhu, J. Wang, S. Sun, and X. You, "Mutual coupling calibration for multiuser massive MIMO systems," *IEEE Trans. on Wireless Commun.*, vol. 15, no. 1, pp. 606–619, 2016.
- [14] R. Rogalin, O. Y. Bursalioglu, H. C. Papadopoulos, G. Caire, and A. F. Molisch, "Hardware-impairment compensation for enabling distributed large-scale MIMO," in *2013 Information Theory and Applications Workshop (ITA)*. IEEE, 2013, pp. 1–10.
- [15] 3GPP, "Evolved universal terrestrial radio access (E-UTRA); physical channels and modulation," 3GPP, Tech. Rep. Technical Specification 36.211 V15.2.0 Release 15, October 2018.